Applied Catalysis B: Environmental 165 (2015) 438–445

Contents lists available at ScienceDirect

Applied Catalysis B: Environmental

journal homepage: www.elsevier.com/locate/apcatb

A comparison of hydrothermal aging effects on NH_3-SCR of NO_x over Cu-SSZ-13 and Cu-SAPO-34 catalysts

Di Wang[a,b], Yasser Jangjou[a], Yong Liu[a], Munish K. Sharma[a], Jinyong Luo[b], Junhui Li[b], Krishna Kamasamudram[b], William S. Epling[a,*]

[a] University of Houston, Department of Chemical and Biomolecular Engineering, 4800 Calhoun Rd., Houston, TX 77204-4004, USA
[b] Cummins Inc, 1900 McKinley Ave, Columbus, IN 47201, USA

ARTICLE INFO

Article history:
Received 23 August 2014
Received in revised form 5 October 2014
Accepted 7 October 2014
Available online 16 October 2014

Keywords:
NH_3-SCR
SAPO-34
SSZ-13
Hydrothermal aging.

ABSTRACT

The impacts of hydrothermal aging on the selective catalytic reduction (SCR) performance of both Cu-SSZ-13 and Cu-SAPO-34 were compared. Upon 750 °C hydrothermal aging for 16 h, the NO conversions on both materials were somewhat maintained, however, a significant difference appeared after hydrothermal aging at 800 °C. The Cu-SSZ-13 sample resulted in remarkably lower NO conversions at all temperatures tested while the Cu-SAPO-34 still maintained its high SCR activity. In fact, the NO conversions at low temperatures (below 350 °C) over Cu-SAPO-34 were even enhanced upon high temperature treatment, suggesting an increase in active sites, which is possibly due to a post solid state ion exchange process driven by high temperatures. Consistently, for the Cu-SAPO-34 sample, NH_3-TPD results suggest an increase in Lewis acid sites after hydrothermal aging at 750 and 800 °C as compared with the fresh one. However, for the Cu-SSZ-13 sample, DRIFTs characterization results suggest a decrease in acid sites (Brønsted and Lewis), and a significant reduction in the amount of exchanged Cu^{2+} sites upon aging at 800 °C, leading to a drastically decreased SCR activity. XRD results also showed the CHA (chabazite) structure collapses for Cu-SSZ-13 after 800 °C hydrothermal aging of Cu-SSZ-13, but still remains for Cu-SAPO-34 upon the same aging. Besides SCR performance, critical functions of the SCR catalyst including NH_3 oxidation activity and selectivity to NO_x were also evaluated. Over Cu-SSZ-13, initial aging at 750 °C results in increased NH_3 oxidation and selectivity to NO_x, suggesting the aggregation of isolated Cu^{2+} sites into CuO particles, while further aging at 800 °C leads to decreased NH_3 oxidation activity due to structure collapse as evidenced by XRD. On the other hand, for Cu-SAPO-34, no significant change in NH_3 oxidation was observed after hydrothermal aging. All SCR performance test, NH_3 oxidation and characterization results consistently indicate that Cu-SAPO-34 is more robust than Cu-SSZ-13 towards hydrothermal aging for the formulations and conditions examined here.

1. Introduction

There has been recent significant interest in more widespread use of lean burn diesel engines due to better fuel economy and greater power density compared to conventional gasoline engines. However, to meet regulations, their use depends on the effective reduction of two primary diesel exhaust components: nitrogen oxides (NO_x) and particulate matter (PM). The selective catalytic reduction of NO_x by NH_3 (NH_3-SCR) is one of the most promising NO_x abatement technologies. In a typical NH_3-SCR after-treatment system, a diesel oxidation catalyst (DOC) and diesel particulate filter (DPF) are used to remove the unburned hydrocarbons, CO and particulate matter upstream of the SCR catalyst. The DPF needs to be periodically regenerated and a great deal of heat might then be transferred to the SCR catalyst. The high-temperature exposure (>650 °C) with the presence of moisture in the feed could damage the zeolite framework structure and lead to catalyst deactivation. Therefore, the resistance to hydrothermal aging can be crucial for NH_3-SCR catalyst application. Both Fe- and Cu-exchanged zeolite frameworks with medium and large pores, such as MFI (ZSM-5), FER and BEA, have been evaluated and considered as SCR catalyst candidates [1]. However, the hydrothermal stability of these catalysts was/is problematic [2,3]. In the last several years, small-pore Cu-exchanged Chabazite (Cu-CHA) catalysts, such as Cu-SAPO-34 and Cu-SSZ-13, were discovered and commercialized by researchers from BASF and Johnson Matthey [4]. One of the

* Corresponding author. Tel.: +1 713 743 4234.
E-mail address: wsepling@uh.edu (W.S. Epling).

http://dx.doi.org/10.1016/j.apcatb.2014.10.020
0926-3373/

significant advantages of the small-pore Cu-CHA zeolite catalysts is the excellent hydrothermal stability. Both Cu-SSZ-13 and Cu-SAPO-34 are reported to maintain their SCR activity after hydrothermal aging at 800 °C [2,3,5,6]. SSZ-13 and SAPO-34 zeolites have their largest pore opening of 3.8 Å. The dealumination product $Al(OH)_3$, which has a calculated kinetic diameter of 5.03 Å, is likely to be restrained in the small pores and as a result, the dealumination process is hindered during the hydrothermal aging process [2]. Meanwhile, different types/locations of Cu structures have been observed on Cu-CHA catalysts, such as isolated Cu^{2+}, Cu^{+}, Cu dimers $(Cu–O–Cu)^{2+}$, Cu_xO_y clusters, and CuO particles [2,7–11]. Recently, Kim et al. found that these Cu species have different resistances to the hydrothermal aging process. Particularly, Cu species occupying the CHA sites were found to be less stable than the Cu^{2+} species in the D6R unit, therefore, the authors believed the former structure is primarily responsible for the hydrothermal aging of Cu-SSZ-13 catalysts [12]. In addition, Ma et al. found that Cu migration, acidity loss and dealumination occurred on both Cu-SAPO-34 and Cu-SSZ-13 catalysts after hydrothermal aging [13]. Fickel et al. [2] observed low-temperature NO conversions increased over SAPO-34-based samples after a hydrothermal aging treatment and this was later explained by the fact the high temperature treatment enabled more Cu to migrate into the pores SAPO-34 [5,13,14]. Interestingly, no such phenomenon was detected with Cu-SSZ-13 [3,13]. The discrepancies between SSZ-13 and SAPO-34 upon hydrothermal aging are still not clear. Therefore, the objective of the present study is to investigate the hydrothermal aging effects on Cu-SSZ-13 and Cu-SAPO-34 catalysts. XRD, DRIFTS and NH_3-TPD were used to characterize the structure, acidity and Cu site changes during the hydrothermal treatment. Different resistances to hydrothermal aging are discussed.

2. Experimental methods

2.1. Catalyst preparation and hydrothermal aging

The H-form SAPO-34 zeolite support with an (Al + P)/Si ratio of 5 was purchased from ACS materials. The Na-form SSZ-13 zeolite was synthesized by PNNL using the hydrothermal method described in Ref [2]. The obtained Na-SSZ-13 zeolite has a Si/Al ratio of 6. It is worth noticing here that the (Al + P)/Si on SAPO-34 and Si/Al on SSZ-13 are close enough to hypothetically eliminate their influence on the hydrothermal stability of the two materials. Subsequently, Na-SSZ-13 was added into a 0.1 M NH_4NO_3 solution with continuous stirring at 80 °C for 8 h. The resulting NH_4-SSZ-13 powder was separated from the solution by filtration followed by several washing steps. Finally, the material was dried in an oven at 120 °C overnight. The solid-state ion exchange was performed in a tube furnace equipped with a continuous flow of air. The detailed procedure is described in Ref [15]. Both SAPO-34 and SSZ-13 were heated at 700 °C in the presence of 350 cm^3/min dry air for 16 h. The as-prepared samples are named as SS-CuSSZ-13(700C) and SS-CuSAPO-34(700C), respectively. The hydrothermal aging was performed with the presence of 10% O_2 and 10% H_2O with a total flow of 600 cm^3/min, corresponding to a gas hourly space velocity (GHSV) of 240,000 h^{-1}. Both of the catalysts were progressively aged at 750 and 800 °C for 16 h, respectively.

2.2. Catalyst characterization

The elemental compositions of the samples were analyzed by ICP (Galbraith Laboratories). The resulting Cu loadings on the two samples were 3.97% on SAPO-34 and 4.10% on SSZ-13. X-ray diffraction (XRD) measurements were performed in a Siemens D5000 Diffractometer equipped with a Cu Kα detector. Transmission electron microscope (TEM) images were obtained by a JEOL 2000 FX TEM machine at an accelerating voltage of 200 keV and 2.8 Å resolution. The particle sizes were estimated using image processing and analysis software Image J (a Java-based image processing program developed at the National Institutes of Health). The NH_3 temperature-programmed desorption (NH_3-TPD) experiments were conducted in a micro-scale reactor system and the NH_3 effluent concentration was measured by FTIR (MultiGas 2030). In each test, 120 mg of the powder catalyst sample was diluted with 360 mg quartz beads in order to obtain a better distribution of the catalyst particles and reduce the pressure drop in the catalyst bed. The pretreatment was performed with 10% O_2 in N_2 at 550 °C for 1 h. After pretreatment, a total flow of 300 cm^3/min containing 500 ppm NH_3 in N_2 was introduced into the reactor for 2 h at 35 °C. After the catalyst was saturated, NH_3 was switched off and only N_2 was fed to the reactor for another 2 h to remove any gas-phase or weakly adsorbed NH_3. The final stage involved a temperature ramp to 550 °C with a heating rate of 10 °C/min. In-situ DRIFTS experiments were performed using a Nicolet 6700 spectrometer equipped with a high-temperature reaction chamber (Harrick Praying Mantis). In each DRIFTS experiment, 60 mg of powder catalyst was loaded into the sample cup of the high-temperature reaction chamber. The pretreatment was conducted at 550 °C in 10% O_2/He for 1 h before cooling to 30 °C. For NH_3 and NO adsorption experiments, the spectra were taken by subtracting the background spectra recorded during exposure to the sample to 50 cm^3/min pure He. NH_3 adsorption was conducted in a 50 cm^3/min flow containing 500 ppm NH_3 in a balance of He and NO adsorption spectra were performed in a 50 cm^3/min flow containing 200 ppm NO in a balance of He.

2.3. NH_3-SCR and NH_3 oxidation reaction tests

The standard SCR reaction and NH_3 oxidation reaction tests were performed by loading 120 mg powder catalyst (40–60 mesh) mixed with 360 mg quartz beads in the micro-scale reactor. Prior to each test, the catalyst was pretreated at 550 °C for 2 h in flowing 10% O_2 in a balance of N_2. The simulated exhaust gas contained 500 ppm NO, 500 ppm NH_3, 10% O_2 and 10% H_2O with a balance of N_2. The NH_3 oxidation reaction tests were carried out in a flow of 500 ppm NH_3, 10% O_2 and 10% H_2O with a balance of N_2. The water vapor for the feed was supplied by a Bronkhorst CEM liquid delivery system. All the lines are heated and maintained at 130 °C to prevent any condensation. The effluent gas concentration was measured with a MultiGas 2030 FTIR spectrometer. The total flow rate was 600 cm^3/min and the corresponding GHSV was 240,000 h^{-1}. The NO and NH_3 conversions were calculated using the following equations:

$$X_{NO} = \frac{C_{NO_{x_{in}}} - C_{NO_{x_{out}}}}{C_{NO_{in}}} \times 100\%$$

and

$$X_{NH_3} = \frac{C_{NH_{3_{in}}} - C_{NH_{3_{out}}}}{C_{NH_{3_{in}}}} \times 100\%$$

3. Results and discussion

3.1. SCR performance

The SCR performance results of SS-CuSSZ-13(700C) and SS-CuSAPO-34(700C) before and after the hydrothermal aging are shown in Figs. 1 and 2, respectively. Both fresh Cu-SSZ-13 and Cu-SAPO-34 samples show good SCR activity over the range of temperatures used. In particular, over 90% NO conversion between 300 and 450 °C was achieved on both samples. The fresh Cu-SSZ-13

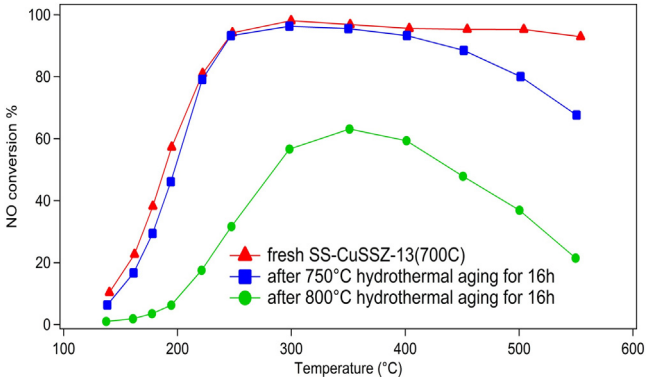

Fig. 1. SCR performance for SS-CuSSZ-13(700C) before and after 750 or 800 °C hydrothermal aging for 16 h (aging conditions: 10% H_2O, 10% O_2, balance N_2, GHSV = 240,000 h^{-1}).

sample maintained its high activity at temperatures above 450 °C. However, the Cu-SAPO-34 showed slightly lower NO_x conversions at temperatures above 450 °C. Both fresh samples resulted in high N_2 selectivity (near 100%) and no NH_3 slip. After 750 °C hydrothermal aging for 16 h, the low-temperature SCR activity (<200 °C) only slightly dropped on Cu-SSZ-13, while the NO conversions at temperatures higher than 400 °C more significantly decreased. On the other hand, the NO conversion at low temperature increased with the Cu-SAPO-34 sample. The NO conversion significantly dropped for Cu-SSZ-13 after hydrothermal aging at 800 °C for 16 h, which was also accompanied by some NH_3 slip from the catalyst. For example, the maximum NO conversion was observed to be 63% at 350 °C, corresponding to a 30% reduction from that obtained with the fresh sample. In comparison, most of the SCR activity was maintained and still no NH_3 slip was detected over Cu-SAPO-34 after the same aging process, where only a slight drop in the NO conversion was observed over the test temperature range. Therefore, it seems that the Cu-SAPO-34 sample was more resistant to hydrothermal aging than Cu-SSZ-13, at least under the applied aging conditions.

3.2. NH_3 oxidation

The NH_3 oxidation activity and selectivity was tested over the Cu-SSZ-13 and Cu-SAPO-34 samples before and after the hydrothermal aging. As shown in Fig. 3, NH_3 oxidation started at 300 °C and increased with increasing temperature on the fresh SS-CuSSZ-13(700C) sample. After 750 °C hydrothermal aging, the NH_3 conversion increased, with 100% NH_3 conversion at 550 °C, which was also accompanied by a significant increase in NO_x selectivity, as

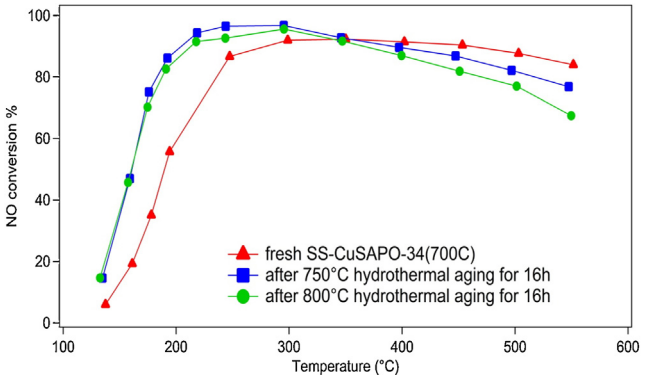

Fig. 2. SCR performance for SS-CuSAPO-34(700C) before and after 750 or 800 °C hydrothermal aging for 16 h (aging conditions: 10% H_2O, 10% O_2, balance N_2, GHSV = 240,000 h^{-1}).

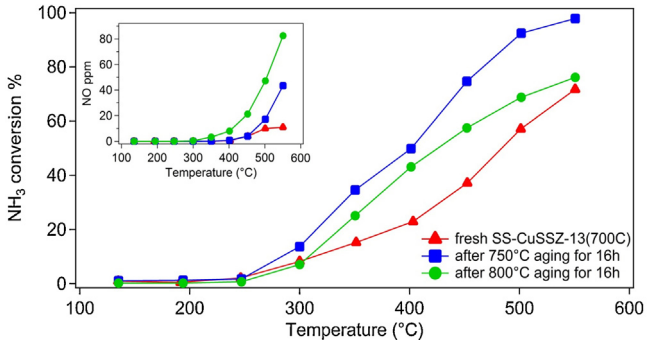

Fig. 3. NH_3 conversions during NH_3 oxidation reaction on SS-CuSSZ-13 (reaction conditions: 500 ppm NH_3, 10% H_2O, 10% O_2, balance N_2, GHSV = 240,000 h^{-1}).

shown in the inset. The increased NH_3 conversion and NO_x selectivity via non-selective NH_3 oxidation could explain the drop in NO conversion in standard SCR tests after 750 °C hydrothermal aging. With further hydrothermal treatment at 800 °C, the NO_x selectivity continued to increase, however, the NH_3 oxidation activity dropped, which could be due to the fact that the surface area and pore structure were severely damaged at this aging condition and therefore the catalytic activity was significantly hindered (as discussed below). On the other hand, after 750 and 800 °C hydrothermal aging, no such significant change in the NH_3 conversion, as well as the NO selectivity, were observed with Cu-SAPO-34 as shown in Fig. 4. Actually, the hydrothermally aged Cu-SAPO-34 presented slightly higher NH_3 conversion, however, the degree of this increasing trend is much less than what was observed on Cu-SSZ-13 samples. It is also worth noting that the NH_3 conversion in tests with the fresh SS-CuSAPO-34(700C) was much higher than that with fresh SS-CuSSZ-13(700C) (Fig. 3).

3.3. Characterization of the catalysts

3.3.1. Structural properties

In order to probe the structural changes during the hydrothermal aging process over Cu-SAPO-34 and Cu-SSZ-13 samples, XRD measurements were taken using samples before and after the hydrothermal treatment. As shown in Fig. 5, the crystallinity of fresh SS-CuSSZ-13(700C) was well maintained after the solid state ion exchange process as all the diffraction peaks related to CHA phases (marked by dashed lines) were observed in the XRD pattern. After 750 °C hydrothermal aging, some of the Cu-SSZ-13 crystallinity features disappeared in the XRD pattern, which could be explained by some structural damage caused by the hydrothermal aging. In addition, a broad peak was observed in the 2 theta range of 10–20° due to the reduction in the intensity of destructive interference. This further supports the formation of some

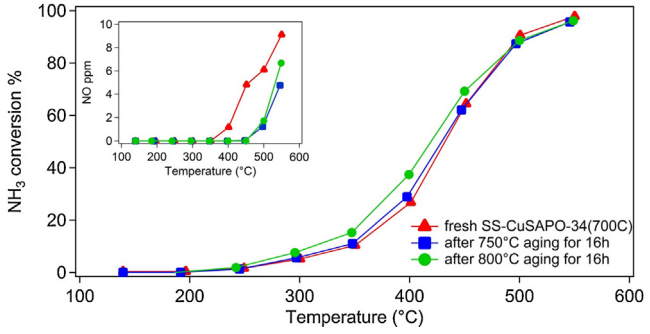

Fig. 4. NH_3 conversions during NH_3 oxidation reaction on SS-CuSAPO-34 (reaction conditions: 500 ppm NH_3, 10% H_2O, 10% O_2, balance N_2, GHSV = 240,000 h^{-1}).

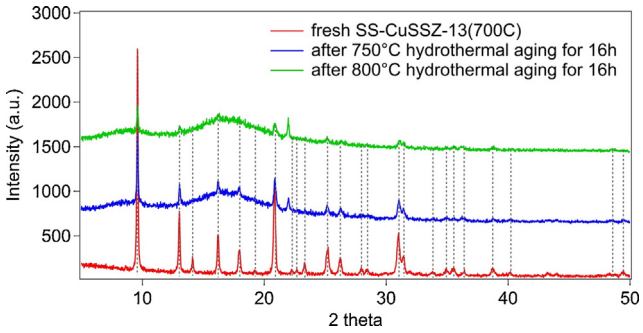

Fig. 5. XRD patterns of as-prepared SS-CuSSZ-13(700C) samples before and after hydrothermal aging at 750 or 800 °C.

amorphous phases that formed during the hydrothermal aging process. 800 °C hydrothermal aging resulted in an even more dramatic collapse of the crystal structure of Cu-SSZ-13. This is evidenced by the loss of more CHA related features in the XRD pattern. In summary, more significant structural damage of the zeolite framework was detected as the hydrothermal aging temperature increased from 750 to 800 °C, which corresponds to the dramatic drop in NO conversion during SCR tests with Cu-SSZ-13 sample after 800 °C hydrothermal aging.

The XRD patterns of SS-CuSAPO-34(700C) before and after hydrothermal aging are shown in Fig. 6. Sharp diffraction peaks, which correspond to the CHA phases, were obtained on the fresh Cu-SAPO-34 sample. These crystal phases were very well maintained after hydrothermal aging at 750 °C as evidenced by the lack of disappearance of diffraction peaks. In addition, a broad peak, which may originate from some amorphous phase, was also detected on Cu-SAPO-34. When the aging temperature was increased to 800 °C, there was still no significant loss of the crystallinity detected on Cu-SAPO-34 material. This further proves that Cu-SAPO-34 structure was indeed more robust than Cu-SSZ-13.

The TEM images obtained that describe the evolution of as-prepared SS-CuSSZ-13(700C) and SS-Cu-SAPO-34(700C) samples during the hydrothermal aging process are shown in Fig. 7. The particle sizes of the fresh SSZ-13 and SAPO-34 crystals were observed to be around 100–200 nm. In addition, some small particles with average sizes of 2.35 and 2.18 nm were observed in the fresh SS-CuSSZ-13(700C) and SS-CuSAPO-34(700C), respectively. These particles are believed to be residual CuO particles, from the synthesis, as EDX elemental analysis showed the presence of Cu in these particles. The presence of CuO particles indicates that the solid-state ion exchange process was not completely accomplished therefore some un-exchanged CuO remained located outside the pores of the zeolite. After the hydrothermal aging at 750 °C, the average particle sizes of the CuO in SSZ-13 and SAPO-34 increased to 3.97 and 4.57 nm, respectively. With a further increase in the

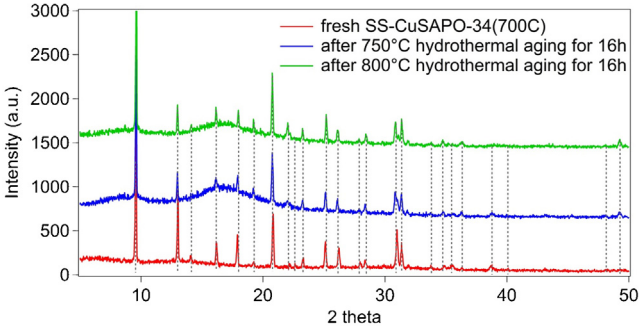

Fig. 6. XRD patterns of as-prepared SS-Cu-SAPO-34(700C) samples before and after hydrothermal aging at 750 or 800 °C.

aging temperature to 800 °C, the CuO particles continued to aggregate and the particle sizes grew to 4.43 and 9.28 nm on SSZ-13 and SAPO-34, respectively.

3.3.2. NH_3-TPD

NH_3 temperature-programmed desorption (NH_3-TPD) experiments were conducted in order to investigate acidity evolution during the hydrothermal aging process. Fig. 8 shows the NH_3 profile collected during the temperature ramp over SS-CuSSZ-13(700C). Three peaks were observed on the fresh sample: a low-temperature peak at 150 °C, a high-temperature peak above 400 °C and a smaller feature between these low- and high-temperature peaks at around 280 °C. Based on analysis in our previous studies [15,16], the low-temperature peak at 150 °C is assigned to weakly adsorbed NH_3, such as physisorbed NH_3 and NH_3 adsorbed on weak Lewis acid sites. The desorption peak at 280 °C and the high-temperature peak above 400 °C are associated with NH_3 adsorbed on strong Lewis acid sites, which are created by the exchanged Cu ions, and Brønsted acid sites, respectively. After 750 °C hydrothermal aging, all the NH_3 desorption peaks were reduced, indicating that both the Brønsted and Lewis acid sites were lost due to the hydrothermal aging. Furthermore, the 800 °C hydrothermal treatment resulted in a more significant reduction of the number of acid sites.

In comparison, the NH_3 profile during the TPD taken over SS-CuSAPO-34(700C) also showed three similar desorption peaks (Fig. 9). Interestingly, the high-temperature desorption peak corresponding to the NH_3 desorbed from Brønsted acid sites was more intense on Cu-SAPO-34 than that on Cu-SSZ-13. This might be explained by the fact that the Cu-SAPO-34 is more robust to dealumination, which may have already taken place during the high-temperature treatment of the solid-state synthesis process, therefore resulting in much less loss of the Brønsted acid sites on Cu-SAPO-34. Surprisingly, the intensity of the 280 °C NH_3 desorption peak, which corresponds to NH_3 adsorbed on the Lewis acid sites, increased after hydrothermal aging at 750 and 800 °C. This strongly indicates that Cu ions continued to migrate and exchange with protons during the hydrothermal treatment on Cu-SAPO-34. As a result, the number of Lewis acid sites that were created by exchanged Cu sites increased. Indeed, the increasing number of exchanged Cu sites after the hydrothermal aging could be responsible for the enhanced low-temperature SCR activity that was observed with the Cu-SAPO-34 sample. However, this result was not observed on the NH_3-TPD profiles taken over Cu-SSZ-13.

3.3.3. DRIFTS-NH_3 adsorption

In order to further investigate the different hydrothermal aging effects, in-situ DRIFTS experiments were used to characterize the different Cu sites. First, NH_3 was used as a probe molecule since NH_3 can adsorb on both Brønsted acid sites and Lewis acid sites of the zeolite material. Therefore, the relative intensities of the DRIFTS spectra features after NH_3 saturation are indicative of the total amounts of different acid sites. The DRIFTS spectra taken after NH_3 saturation of the SS-CuSSZ-13(700C) sample are shown in Fig. 10. Several negative bands at 3733, 3660, 3640, 3612 and 3585 cm^{-1} were observed in the spectra. The bands in this area are typically assigned to OH stretching vibrations on the zeolite surface. These bands were negative due to weakened vibrations caused by NH_3 adsorption on the OH groups. For example, the band at 3733 cm^{-1} is due to the NH_3 adsorbed on the external Si-OH sites [17]. And the bands at 3640 and 3660 cm^{-1} are tentatively assigned to NH_3 adsorbed on the Al-OH and Cu-OH groups, respectively [17–22]. The bands at 3612 and 3585 cm^{-1} correspond to the stretching vibrations of the Al–OH–Si groups, which are signatures of Brønsted acid sites on CHA materials [17,23,24]. After hydrothermal aging at 750 °C, all of these bands were less intense, which is again due to the structural collapse caused by the hydrothermal aging. This

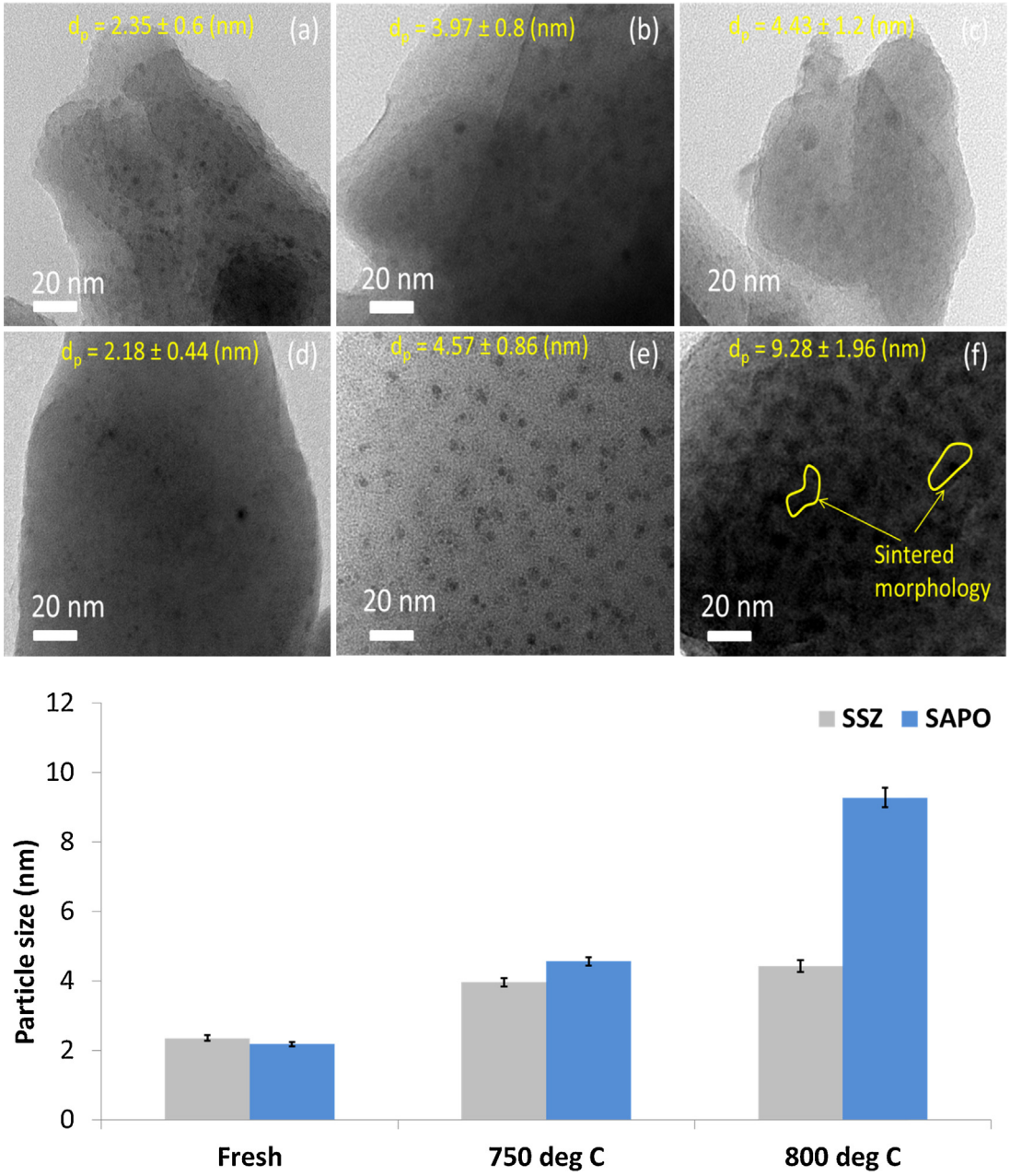

Fig. 7. TEM images on as-prepared SS-CuSSZ-13(700C) and SS-Cu-SAPO-34(700C) samples before and after hydrothermal aging at 750 or 800 °C: (a) fresh Cu-SSZ-13; (b) 750 °C aged Cu-SSZ-13; (c) 800 °C aged Cu-SSZ-13; (d) fresh Cu-SAPO-34; (e) 750 °C aged Cu-SAPO-34; (f) 800 °C aged Cu-SAPO-34.

reduction is more significant after the sample was hydrothermally aged at 800 °C. As shown in Fig. 10, almost no OH stretching vibrations could be identified in the DRIFTS spectra taken after NH_3 adsorption, demonstrating a loss in surface OH groups after hydrothermal aging.

An intense negative band was detected at 900 cm^{-1} and was accompanied by a weak shoulder at 940 cm^{-1}. The peaks in this region are assigned to the tetrahedral cation-oxygen-tetrahedral cation (T-O-T) framework vibrations that were perturbed by ion exchanged copper species [25]. These bands are negative due to the restored T-O-T vibrations with NH_3 adsorption on the Cu sites, confirming the existence of two different exchanged copper species. After 750 °C hydrothermal aging, the amounts of these two exchanged copper species were reduced, as compared to the fresh sample. With the increase in the hydrothermal aging temperature from 750 to 800 °C, these two features are barely evident in the spectra, indicating a severe loss in the amount of exchanged Cu sites. This is also consistent with the NH_3-TPD results from the same catalyst showing that the amounts of both Brønsted acid sites and Lewis acid sites decreased after hydrothermal aging.

A different evolution in the surface structural changes was observed in the DRIFTS spectra taken after saturating the SS-CuSAPO-34(700C) sample with NH_3, as shown in Fig. 11. In the OH stretching region, the weak negative band at 3671 cm^{-1} is assigned to the external surface P-OH groups [26]. Two intense negative bands at 3625 and 3600 cm^{-1} originated from the stretching vibrations of bridging OH groups (Al-OH-Si) [26]. 750 °C hydrothermal aging for 16 h resulted in slight decreases in the intensities of the Al-OH-Si groups, hinting at a mild decrease in the amount of Brønsted acid sites. It is also worth noting that the degree of this reduction is much less evident than that observed on the 750 °C hydrothermally aged Cu-SSZ-13 sample. Furthermore, the band intensities

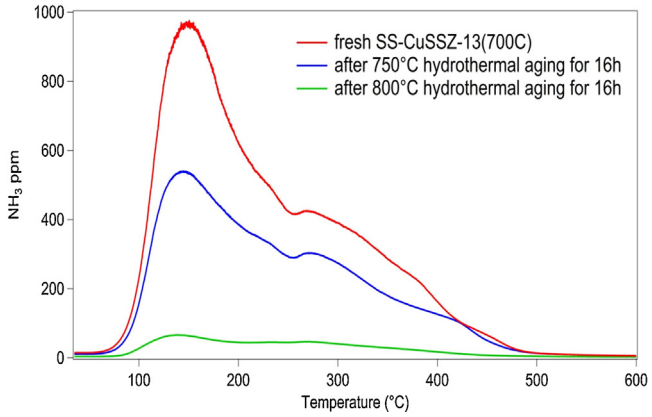

Fig. 8. NH_3-TPD results over SS-CuSSZ-13(700C) sample (500 ppm NH_3 adsorption at 35 °C for 2 h followed by purging by N_2 for 2 h, subsequently the temperature was ramped to 550 °C with a heating rate of 10 °C/min in N_2).

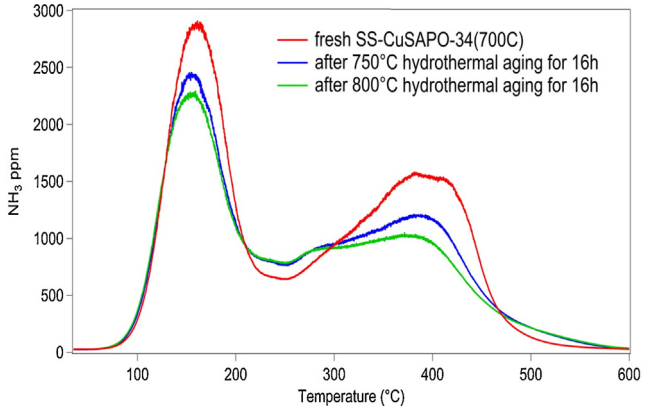

Fig. 9. NH_3-TPD results over SS-CuSAPO-34(700C) (500 ppm NH_3 adsorption at 35 °C for 2 h followed by purging by N_2 for 2 h, subsequently the temperature was ramped to 550 °C with a heating rate of 10 °C/min in N_2).

of Al-OH-Si groups maintained their intensities after 800 °C hydrothermal aging, which was not observed with aged Cu-SSZ-13.

Another distinction between Cu-SSZ-13 and Cu-SAPO-34 can be observed when comparing the exchanged Cu DRIFTS features upon NH_3 adsorption. As shown in Fig. 11, two intense bands with negative intensities were observed at 900 and 850 cm^{-1}. Similar to those detected on the Cu-SSZ-13 sample, these two bands are assigned to the tetrahedral cation-oxygen-tetrahedral cation (T-O-T) framework vibrations that were perturbed by ion exchanged copper species. Noticeably, the shapes of these Cu features are

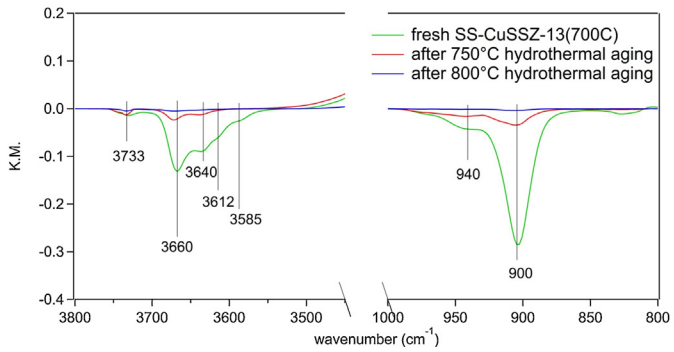

Fig. 10. DRIFTS spectra taken over NH_3 saturated as-prepared SS-CuSSZ-13(700C) sample (experimental conditions: sample exposed to 500 ppm NH_3 in He at 30 °C for 60 min, total flow was 50 cm^3/min).

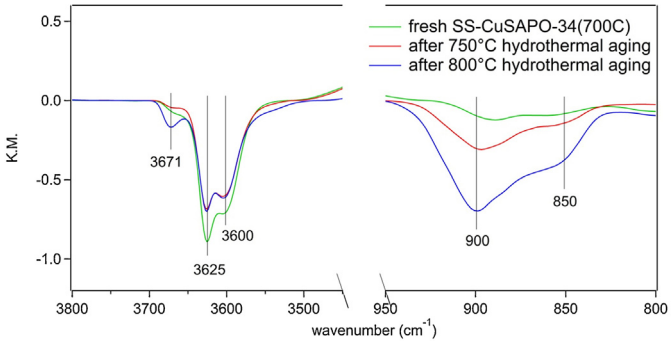

Fig. 11. DRIFTS spectra taken over NH_3 saturated as-prepared SS-CuSAPO-34(700C) sample (experimental conditions: sample exposed to 500 ppm NH_3 in He at 30 °C for 60 min, total flow was 50 cm^3/min).

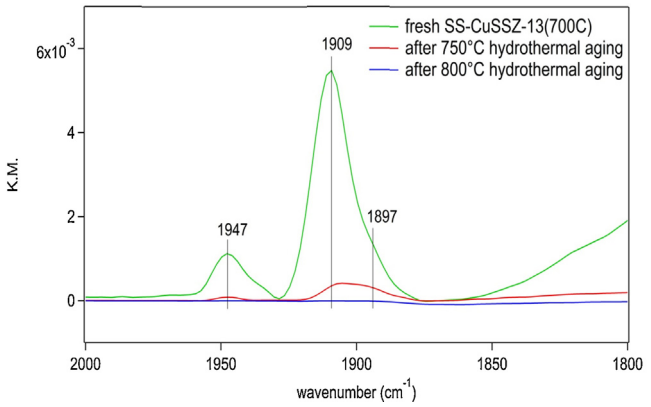

Fig. 12. DRIFTS spectra taken over the NO saturated as-prepared SS-CuSSZ-13(70C) sample (experimental conditions: sample exposed to 200 ppm NO in He at 30 °C for 60 min, total flow was 50 cm^3/min).

distinct upon comparison. For example, the exchanged Cu feature at 900 cm^{-1} (type 2 Cu) is very intense for Cu-SAPO-34 while it was only a shoulder for Cu-SSZ-13. This is explained by the fact that a different type and/or location of Cu site was predominantly formed on the Cu-SAPO-34 sample [25]. This band was previously assigned to be associated with the exchanged Cu_xO_y clusters on the sample. After the 750 °C hydrothermal treatment, both of the exchanged Cu features significantly increased in intensity. This is not surprising since the NH_3-TPD results showed more Lewis acid sites, which were generated by the post solid-state ion exchange of Cu during the hydrothermal aging process. As the hydrothermal aging temperature increased from 750 to 800 °C, Cu migration was more evident as more intense exchanged Cu features were detected with the 800 °C hydrothermally aged sample. Accordingly, the SCR performance was further enhanced on the Cu-SAPO-34.

3.3.4. DRIFTS-NO adsorption

Cu migration during the aging of Cu-SAPO-34 was further confirmed by NO adsorption experiments performed and characterized using DRIFTS. Fig. 12 shows the DRIFTS spectra taken upon exposing the SS-CuSSZ-13(700C) sample to NO. Here, the catalysts were treated with 10% O_2 before NO was introduced, therefore all the surface-exchanged Cu sites are presumed to be in the Cu^{2+} state. During the NO adsorption process, major bands in the range of 1800–2000 cm^{-1} were immediately observed. The band at 1909 cm^{-1}, which was accompanied by the band at 1947 cm^{-1}, is assigned to NO adsorbed on the isolated Cu^{2+} sites [16]. Additionally, the band at 1897 cm^{-1} corresponds to NO adsorbed on another type of Cu^{2+} site, possibly Cu_xO_y clusters [27,28]. Thus, these bands could be the signatures of surface Cu^{2+} sites. After

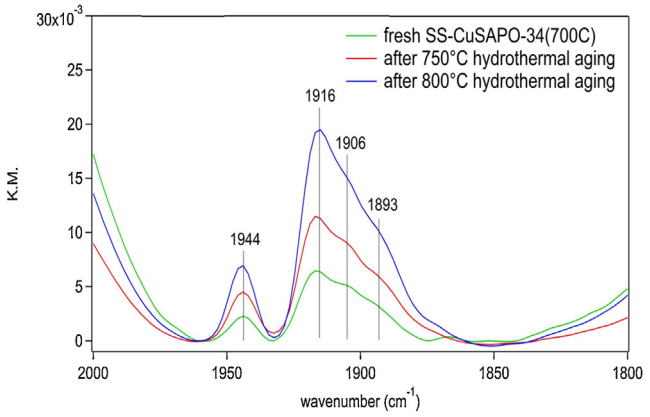

Fig. 13. DRIFTS spectra taken over the NO saturated as-prepared SS-CuSAPO-34(700C) sample (experimental conditions: sample exposed to 200 ppm NO in He at 30 °C for 60 min, total flow was 50 cm^3/min).

750 °C hydrothermal aging, all of these bands decreased for Cu-SSZ-13, proving that the number of Cu^{2+} sites that adsorbed NO dropped after aging. Moreover, these bands were almost absent in the spectra taken from the sample after 800 °C hydrothermal aging. All of these results coincide with the fact that exchanged Cu^{2+} sites were lost by the hydrothermal aging.

The DRIFTS spectra taken after exposing the Cu-SAPO-34(700C) sample to NO are shown in Fig. 13. Several bands were observed, at 1944, 1916, 1906, and 1893 cm^{-1}, upon NO adsorption. Similar to Cu-SSZ-13, these bands correspond to NO that adsorbed on different Cu^{2+} sites [16,18,27]. After 750 °C hydrothermal aging, the band intensities were higher than those observed on the fresh Cu-SAPO-34, indicating that the total amount of Cu^{2+} that adsorbed NO increased after hydrothermal aging. With 800 °C hydrothermal aging, the band intensities again increased, further confirming that more Cu ions were incorporated into the zeolite framework and generated exchanged Cu^{2+} sites. All of these observations coincide with the observations from the NH_3-TPD and NH_3-exposure DRIFTS results showing that Cu-SAPO-34 is resistant to the hydrothermal treatment even at 800 °C. Furthermore, the results show that Cu was still migrating into the pores of Cu-SAPO-34 material via the solid-state ion exchange process. As a result, more isolated Cu^{2+} sites, which are active for the NH_3-SCR reaction, formed on Cu-SAPO-34. For the Cu-SSZ-13 catalyst, hydrothermal aging led to a significant drop in the SCR activity due to severe structural damage. In addition, the initial increase in NH_3 oxidation activity indicates Cu site changes. Indeed, it is likely that some exchanged Cu^{2+} sites detached from the framework and formed CuO particles that consumed additional NH_3 and produced NO_x through the NH_3 oxidation reaction. However, this does not seem to be the case for Cu-SAPO-34, where the NH_3 oxidation activity and selectivity to NO_x was maintained after the hydrothermal aging process.

3.3.5. *Different hydrothermal stabilities of Cu-SSZ-13 and Cu-SAPO-34*

Obviously, Cu-SSZ-13 and Cu-SAPO-34 catalysts have shown very distinct responses to the hydrothermal aging process at 750 and 800 °C. Especially, in the low-temperature region (<250 °C), Cu-SSZ-13 showed consistently decreasing NO conversion after hydrothermal aging at 750 and 800 °C. Simultaneously, the total number of acid sites as well as the amount of exchanged Cu sites significantly dropped, which is evidenced by the NH_3-TPD and in-situ DRIFTS. It seems that some active Cu sites are pulled out of the SSZ-13 framework during the hydrothermal aging process and aggregated into CuO. The exchanged Cu sites have been extensively reported to be the active sites for NH_3-SCR at low temperature [8,10,11,16,26]. After the hydrothermal aging at 800 °C, the low-temperature SCR was impacted by the decreased number of active sites resulting in the significant conversion decrease. Simultaneously, NH_3 slip was observed, providing further evidence for lack in enough active Cu sites. In comparison, no such dramatic loss of the exchanged Cu structure was observed with Cu-SAPO-34. Instead, NH_3-TPD and in-situ DRIFTS results clearly showed that even more exchanged Cu sites were generated after the hydrothermal aging, probably due to a post solid-state ion exchange process. As a result, the low-temperature performance was enhanced by hydrothermal aging of Cu-SAPO-34. The enhancement in the low-temperature performance of Cu-SAPO-34 by thermal or hydrothermal aging has previously been reported elsewhere [5,14,29]. One group of authors attributed it to the formation of additional isolated Cu^{2+} ions during the aging process [29]. Gao et al. reported a 50% loss of the surface area and pore volume of the Cu-SAPO-34 catalysts after 800 °C hydrothermal aging for 16 h. However, more isolated Cu^{2+} ions were indeed formed during this high-temperature treatment and correspondingly, a higher NO_x conversion at low temperature was obtained with the aged sample [5]. Recently, Wang et al. prepared Cu/SAPO-34 using precipitation and wetness ion exchange (WIE) methods and found that after hydrothermal treatment at 700 °C for 48 h, the Cu-SAPO-34 prepared by WIE showed no loss in SCR activity as well as no structural changes. However, the Cu-SAPO-34 prepared by precipitation led to significantly enhanced SCR activity after aging. The XAS analysis conducted by the authors indicated that Cu migration occurred during the high-temperature treatment, which initially involved the formation of metallic Cu followed by re-oxidation of copper ions [14]. All of these findings coincide with our results regarding hydrothermal treatment effects on Cu-SAPO-34. The discrepancy between SSZ-13 and SAPO-34 at low temperature with respect to the hydrothermal aging was also confirmed by XRD results. SSZ-13 lost crystallinity after hydrothermal aging at 800 °C, however, SAPO-34 framework phases remained relatively intact after the same aging condition. Therefore, Cu-SAPO-34 turns out to be more resistant to the hydrothermal aging than the Cu-SSZ-13.

The influence of hydrothermal aging on the high-temperature SCR activity is more complicated. To begin with, the high-temperature SCR activity is closely related to the competitive NH_3 oxidation reaction by O_2 [16,30,31]. Recent studies prove that the NH_3 oxidation reaction follows two steps: (1) formation of NO_x and (2) consumption of NO_x by reacting with the remaining NH_3 through SCR. The selectivity to NO_x in NH_3 oxidation is primarily determined by the relative rate of these two steps [32]. For SSZ-13, the NO_x selectivity in the NH_3 oxidation reaction evidently increased after hydrothermal aging at 750 and 800 °C. The formation of additional NO_x from NH_3 oxidation required more NH_3 for reaction through step (2) and therefore lowered the high-temperature SCR activity of SSZ-13. However, the origin of the change of selectivity in NH_3 oxidation is unclear. For one thing, the aggregation of CuO particles, which is evidenced by TEM, may enhance the NH_3 oxidation selectivity to NO_x [13,30]. Also, the decrease in the number of exchanged Cu sites after hydrothermal aging may hinder step (2), resulting in higher NO_x selectivity over SSZ-13.

For Cu-SAPO-34, the 750 and 800 °C hydrothermal aging led to a relatively moderate decrease in high-temperature NO conversion, which could be explained by the slight increase in NH_3 oxidation activity that challenges the NH_3 availability with increasing aging temperature. Interestingly, for NH_3 oxidation, no such significant change of selectivity was detected on Cu-SAPO-34 regardless of the growth in CuO particle size. This could be related to the fact that step (2) of the NH_3 oxidation was essentially enhanced by the increasing number of exchanged Cu sites.

The origin of the difference in hydrothermal stability between Cu-SSZ-13 and Cu-SAPO-34 still needs further investigation. One of the possible explanations is the different nature of the two types of framework structures. In particular, the SSZ-13 zeolite is crystalline aluminosilicate with a three-dimensional framework built with tetrahedral Si and Al. The Brønsted acidity is mainly derived from the inclusion of Al in the framework, which yields a negative charge that must be counterbalanced by the protons. The Brønsted protons are bound to a bridging oxygen between Al and Si. On the other hand, SAPO-34, a Chabazite-like Zeotype material, is crystalline silicoaluminophosphate whose Brønsted acidity is generated by the substitution of Si in the aluminophosphate structure, initially formed by P and Al. The protons are connected to Al atoms as part of a ligand. The different locations of the protons may lead to possible mechanistic differences in hydrothermal aging [33]. Indeed, it was reported that the crystal structure of SAPO-34 can be maintained up to 1000–1200 °C even in the presence of moisture [34].

4. Conclusions

The hydrothermal stabilities of Cu-SSZ-13 and Cu-SAPO-34 catalysts were characterized and compared. The results show that both Cu-SSZ-13 and Cu-SAPO-34 could maintain their performance with 750 °C hydrothermal aging for 16 h for the formulations and conditions examined here. However, 800 °C hydrothermal aging for 16 h result in a significant reduction of the SCR performance of the Cu-SSZ-13 catalyst, which was accompanied by a drastic loss in crystallinity and active Cu sites. On the other hand, Cu-SAPO-34 did not lose activity with the same aging conditions, but actually the low-temperature NO conversion was increased after the hydrothermal aging. This was explained by residual surface Cu from the original synthesis migrating into the pores of SAPO-34 during the high temperature treatment and forming additional isolated Cu^{2+} sites via the post solid state ion exchange process.

References

[1] M. Iwamoto, H. Furukawa, Y. Mine, F. Uemura, S.I. Mikuriya, S. Kagawa, Journal of the Chemical Society-Chemical Communications (1986) 1272–1273.
[2] D.W. Fickel, E. D'Addio, J.A. Lauterbach, R.F. Lobo, Applied Catalysis B-Environmental 102 (2011) 441–448.
[3] J.H. Kwak, D. Tran, S.D. Burton, J. Szanyi, J.H. Lee, C.H.F. Peden, Journal of Catalysis 287 (2012) 203–209.
[4] US Patent 7, 662 (2009), US Patent 7,704,475 (2010), US Patent 7,998,423 (2011), US Patent 7,998,443 (2011), US Patent 8,101,147 (2012), US Patent 8,182,777 (2012).
[5] F. Gao, E.D. Walter, N.M. Washton, J. Szanyi, C.H.F. Peden, ACS Catalysis (2013) 2083–2093.
[6] Q. Ye, L. Wang, R.T. Yang, Applied Catalysis A: General 427–428 (2012) 24–34.
[7] D.W. Fickel, J.M. Fedeyko, R.F. Lobo, Journal of Physical Chemistry C 114 (2010) 1633–1640.
[8] U. Deka, A. Juhin, E.A. Eilertsen, H. Emerich, M.A. Green, S.T. Korhonen, B.M. Weckhuysen, A.M. Beale, Journal of Physical Chemistry C 116 (2012) 4809–4818.
[9] J.H. Kwak, D. Tran, J. Szanyi, C.H.F. Peden, J.H. Lee, Catalysis Letters 142 (2012) 295–301.
[10] U. Deka, I. Lezcano-Gonzalez, B.M. Weckhuysen, A.M. Beale, ACS Catalysis 3 (2013) 413–427.
[11] J. Xue, X. Wang, G. Qi, J. Wang, M. Shen, W. Li, Journal of Catalysis 297 (2013) 56–64.
[12] Y.J. Kim, J.K. Lee, K.M. Min, S.B. Hong, I.-S. Nam, B.K. Cho, Journal of Catalysis 311 (2014) 447–457.
[13] L. Ma, Y. Cheng, G. Cavataio, R.W. McCabe, L. Fu, J. Li, Chemical Engineering Journal 225 (2013) 323–330.
[14] L. Wang, J.R. Gaudet, W. Li, D. Weng, Journal of Catalysis 306 (2013) 68–77.
[15] D. Wang, F. Gao, C.H.F. Peden, J. Li, K. Kamasamudram, W.S. Epling, ChemCatChem 6 (2014) 1579–1583.
[16] D. Wang, L. Zhang, J. Li, K. Kamasamudram, W.S. Epling, Catalysis Today 231 (2014) 64–74.
[17] L. Sommer, D. Mores, S. Svelle, M. Stocker, B.M. Weckhuysen, U. Olsbye, Microporous and Mesoporous Materials 132 (2010) 384–394.
[18] F. Giordanino, P.N.R. Vennestrom, L.F. Lundegaard, F.N. Stappen, S. Mossin, P. Beato, S. Bordiga, C. Lamberti, Dalton Transactions 42 (2013) 12741–12761.
[19] B. Gil, J. Janas, E. Wloch, Z. Olejniczak, J. Datka, B. Sulikowski, Catalysis Today 137 (2008) 174–178.
[20] I. Lezcano-Gonzalez, U. Deka, B. Arstad, A. Van Yperen-De Deyne, K. Hemelsoet, M. Waroquier, V. Van Speybroeck, B.M. Weckhuysen, A.M. Beale, Physical Chemistry Chemical Physics 16 (2014) 1639–1650.
[21] F. Giordanino, E. Borfecchia, K.A. Lomachenko, A. Lazzarini, G. Agostini, E. Gallo, A.V. Soldatov, P. Beato, S. Bordiga, C. Lamberti, Journal of Physical Chemistry Letters 5 (2014) 1552–1559.
[22] J.H. Kwak, T. Varga, C.H.F. Peden, F. Gao, J.C. Hanson, J. Szanyi, Journal of Catalysis 314 (2014) 83–93.
[23] S. Bordiga, L. Regli, D. Cocina, C. Lamberti, M. Bjorgen, K.P. Lillerud, Journal of Physical Chemistry B 109 (2005) 2779–2784.
[24] H. Zhu, J.H. Kwak, C.H.F. Peden, J. Szanyi, Catalysis Today 205 (2013) 16–23.
[25] J.H. Kwak, H. Zhu, J.H. Lee, C.H.F. Peden, J. Szanyi, Chemical Communications 48 (2012) 4758–4760.
[26] L. Wang, W. Li, G.S. Qi, D. Weng, Journal of Catalysis 289 (2012) 21–29.
[27] J. Szanyi, J.H. Kwak, H. Zhu, C.H.F. Peden, Physical Chemistry Chemical Physics 15 (2013) 2368–2380.
[28] J. Szanyi, J.H. Kwak, R.A. Moline, C.H.F. Peden, Physical Chemistry Chemical Physics 5 (2003) 4045–4051.
[29] J. Wang, T. Yu, X. Wang, G. Qi, J. Xue, M. Shen, W. Li, Applied Catalysis B-Environmental 127 (2012) 137–147.
[30] J.H. Kwak, R. Tonkyn, D. Tran, D. Mei, S.J. Cho, L. Kovarik, J.H. Lee, C.H.F. Peden, J. Szanyi, ACS Catalysis 2 (2012) 1432–1440.
[31] O. Mihai, C.R. Widyastuti, S. Andonova, K. Kamasamudram, J. Li, S.Y. Joshi, N.W. Currier, A. Yezerets, L. Olsson, Journal of Catalysis 311 (2014) 170–181.
[32] J. Wang, Y. Huang, T. Yu, S. Zhu, M. Shen, W. Li, J. Wang, Catalysis Science and Technology 4 (2014) 3004–3012.
[33] T. Fjermestad, S. Svelle, O. Swang, The Journal of Physical Chemistry C 117 (2013) 13442–13451.
[34] Y. Watanabe, A. Koiwai, H. Takeuchi, S.A. Hyodo, S. Noda, Journal of Catalysis 143 (1993) 430–436.